Fluorocyanoesters as Additives for Lithium Ion Battery Electrolytes

Joshua J. Walton,[a] Takumi Hiasa,[b] Hideyuki Kumita,[b] Kazumasa Takeshi[b] and Graham Sandford[a*]*

[a] Department of Chemistry, Durham University, South Road, Durham, DH1 3LE, UK.

[b] Murata Manufacturing Co., Ltd., 1-10-1 Higashikotari, Nagaokakyo-shi, Kyoto 617-8555, Japan.

*Takumi.hiasa@murata.com (T.H.), graham.sandford@durham.ac.uk (G.S)

KEYWORDS. Lithium ion battery; electrolyte additive; fluorination; fluorocyanoester.

ABSTRACT. A range of methyl 2-fluorocyanoester derivatives were synthesized from dimethyl 2-fluoromalonate ester and their efficacy as additives in lithium ion battery (LIB) electrolytes was determined. The role played by the 2-fluorocyanoester additives on battery performance was explored by linear sweep cyclic voltammetry, NMR, GCMS and XPS techniques. For all fluorocyanoester additives studied, initial reduction of the carbonyl group occurs which is then followed by formation of the corresponding radical anion. Possible degradation routes arising from loss of fluoride ion, loss of methyl radicals and cleavage of the αβ carbon-carbon bond were

observed and all affect battery performance. Electrode protection upon addition of fluorocyanoesters to the electrolyte is the main contribution to the improvement of battery stability but improvements on the electrode protection are somewhat offset by free radical processes initiated at the anode. Longer alkyl-chain fluorocyanoesters showed the best LIB improvement with effective cathode protection.

1. INTRODUCTION

Lithium ion battery (LIB) manufacture has developed into a major industry since the first commercial release of an LIB cell in 1991. The high energy density and rechargability of LIBs has enabled the industry to develop into an annual global market projected to be valued at *ca*. $92 billion in 2024, due to extensive use of LIBs in mobile phones and increasing demand in the electric car sector. [1] LIBs with layered $LiCoO_2$ (LCO) as a cathode material and graphite as an anode have been widely used in small portable electronic devices such as laptops and mobile phones. [2] For rapid development and increasing applications of electronic devices, LIBs with higher energy and power density are extremely desirable together with higher operating safety of the cell. Further improvement of traditional LCO cathodes by elevating the charging cut-off voltage has received a lot of attention in industry. Indeed, commercial LCO-based LIBs have recently achieved high voltages up to 4.4 V with a quite stable capacity over 160 mAh g^{-1}. However, a further increase of the charge voltage may lead to decomposition of the electrolyte which is one of the causes of capacity decay and deterioration of the long-term safety of a battery due to out-gassing leading to swelling. Electrolyte additives have been widely investigated as one of the items to improve battery safety while enabling high-energy density and high power. [3-5] In

particular, various nitrile derivatives such as succinonitrile (SN, **1**, Figure 1) [6] and other longer chained di-nitriles [7-8] have been found to reduce the irreversible capacity and significantly reduce gas generation within the cell, with SN **1** showing the most pronounced and commercially valuable effect.

Organic molecules bearing fluorine atoms have been used in many applications within the materials sector and, recently, various fluorinated additives have been assessed in LIB electrolyte systems (Figure 1). Probably, one of the most important functions of an additive is to form a solid electrolyte interphase (SEI) layer on the surface of an electrode providing protection for the electrode which prevents degradation through redox reactions, [9,10] helping to prolong battery lifetimes by improved stability of the battery. Highly electronegative fluorine atoms reduce the reduction potential of an organic system which may lead to more rapid, stable SEI formation and, consequently, various additives based on fluoromalonate structures have been synthesized and assessed in LIB systems recently. The *bis*(fluoromalonato)borate ionic liquid additive **2** takes part in SEI formation producing a layer that improves cycle stability and protects the graphite electrode. [11] *bis*(Trimethylsilyl)-2-fluoro-2-methyl-malonate **3** functioned particularly well as a reductive additive because, upon first charge, Hydrogen fluoride (HF) is eliminated and the remaining organic component can be incorporated into the SEI resulting in a thinner layer that protects the battery from detrimental side reactions. [12]

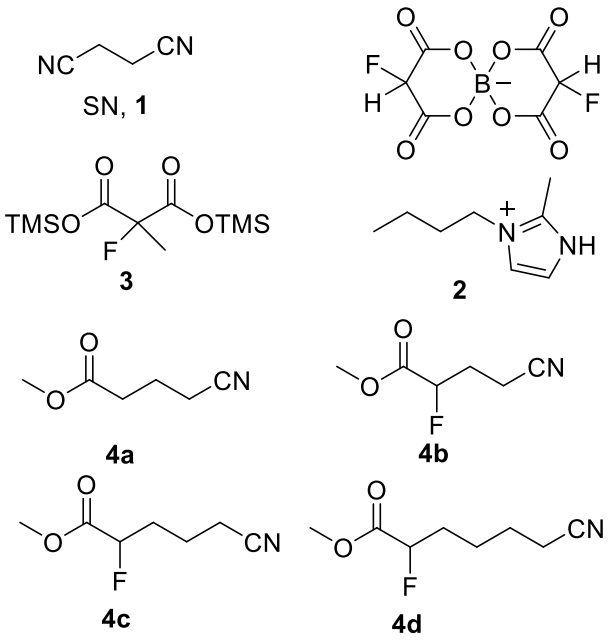

Figure 1. Fluorine containing additives and synthetic targets **4**.

In this paper, we report the synthesis and effect on LIB performance of a range of fluorocyanoester derivatives **4**. The design of this new family of additives aimed to provide a system consisting of a combination of a readily reduced fluoroester functionality and nitrile functionality. Following the synthesis of the fluorocyanoester additives, our aims were to assess how the structural features of the additives (fluoroester, nitrile and the interconnecting alkyl chain) affect SEI layer formation and subsequent gas swelling.

2. MATERIALS AND METHODS

2.1 LIB cell evaluation

The base electrolyte solution was prepared by dissolving 1 mol/kg of $LiPF_6$ salt into the solvent that consisted of a mixture of ethylene carbonate (EC) and propylene carbonate (PC) in a 1:1 weight ratio, followed by the addition of 1 wt% of vinylene carbonate (VC). Materials were battery grade and obtained from Tomiyama Pure Chemicals Industries (Japan) and used without further purification. Methyl cyanobutanoate (MCB **4a**) was purchased from Sigma-Aldrich whilst fluorocyanoesters methyl 4-cyano-2-fluorobutanoate (F-MCB **4b**), methyl 5-cyano-2-fluoropentanoate (F-MCP **4c**) and methyl 6-cyano-2-fluorohexanoate (F-MCH **4d**) were synthesized as described in section 3.1. The additive materials were added to the base electrolyte solution in 1 wt% respectively.

Battery investigations were carried out using coin-type and pouch type cells depending on the experiment. Cathode electrodes were prepared by mixing lithium cobalt oxide ($LiCoO_2$; LCO) with a small amount of conductive carbon additive and poly-vinylidene fluoride (PVDF) binder dispersed in *N*-methyl pyrrolidinone (NMP), and the resulting paste was applied to an aluminum foil current-collector and then dried at 120 °C under vacuum overnight. Anode electrodes were prepared by mixing graphite as the active material in the same way and the resulting paste was applied to a copper foil current-collector and dried at 200 °C under vacuum overnight. The cells were assembled where a polyethylene separator of 20 μm thickness was placed between the two electrodes and each electrolyte solution containing the additive was injected into the assembled cell.

Cell performance was evaluated using a commercial battery tester (TOSCAT, Toyo System Co., Ltd.). The cells were first charged at a constant current density 0.1 C to 4.45 V and constant voltage until the current reached 1/50 C at room temperature. The cells were discharged at a constant current density 0.2 C to 3.0 V to determine the initial capacity of the cell. Then the cell was charged

to 4.45 V again and charged at constant voltage at 4.45 V at 60 °C. After 240 h of constant voltage charging, some cells were discharged to 3.0 V and then the same charge/discharge test as the 1st cycle was performed to determine the capacity retention after aging.

Linear sweep voltammetry was performed using a multichannel potentio-galvanostat (Bio-Logic Science Instrument VMP3) and impedance measurements were conducted using a frequency response analyzer (Solartron 1260) with an electrochemical interface (Solartron SI 1287) in the frequency range of 0.1 Hz to 1 MHz. Z-plot software was employed for data analysis.

2.2 Characterization of SEI layers

Test cells were disassembled in an Ar filled glovebox to prevent samples from moisture/air exposure for post analysis. XPS and NMR analysis were performed to determine surface composition of the electrodes. Electrodes were taken from the disassembled test cell and washed with DMC unless otherwise noted.

2.2.1 X-ray photoelectron spectroscopy (XPS)

The electrode was transferred to an XPS spectrometer (JEOL JPS-9010MX) by a transfer chamber. XPS analyses were carried out using focused monochromatized Al-Ka radiation (1486.6 eV).

2.2.2 Nuclear Magnetic Resonance (NMR)

NMR analysis was carried out to determine the SEI and electrolyte components that resulted from reactions of additives within the cells. Electrodes were collected as mentioned above, rinsed with acetone-d_6, and soaked in deuterated water to extract SEI components. The resulting deuterated aqueous and acetone-d_6 solutions were transferred to NMR tubes and ^{1}H and ^{19}F-NMR analysis

was carried out (JEOL ECA – 500 MHz). Resonances were calibrated with sodium 3-(trimethylsilyl)-[2,2,3,3-d_4]-propanoate (TPS) and lithium bis(trifluoromethanesulfonyl)imide (LiTFSI), respectively. The acquired data was processed by commercial software (ALICE2).

2.2.3 Electrolyte composition

The tested cells were immersed in sufficient DMC to extract electrolyte and the composition of the extracted solution was determined using gas chromatography (Shimadzu GC-20), coupled to a single quadrupole mass spectrometer (Shimadzu QP2020). One drop of extracted electrolyte was added to a 20 mL glass vial and placed on the head-space sampler (Shimadzu HP-20) heated to 250 °C. The GC used a split injection with helium as the carrier gas and equipped with a carbowax-type column (Stabilwax, 30 m, internal diameter 0.35 mm, internal coating 1 μm). The oven temperature ramped from 40 °C to 250 °C at a rate of 20 °C/min. Total ion mass scan was performed to identify and quantify each electrolyte component by retention time and ion ratios of mass spectrum except DMC for extraction. A calibration curve was used to determine the relative amounts of each components, performed using commercial software (Shimadzu LabSolutions).

2.2.4 Gas analysis

Gas mixtures generated during the continuous charging test was collected by a syringe directly from the pouch type cell and was analyzed using an accumulated microGC system (Agilent MicroGC490) equipped with two parallel columns; Molsieve 5A for separation of hydrogen, carbon monoxide, methane, and PoraPLOT Q for separation of carbon dioxide and other volatile hydrocarbons. A calibration curve was calculated using a standard gas of each component and was used to determine the relative composition of the generated gas mixture.

3. RESULTS AND DISCUSSION

3.1 Synthesis of fluorocyanoester compounds **4b-d**

Cyanoester **4a** was used as a reference compound and purchased from commercial suppliers. The fluorocyanoester additive candidates **4b-d** were synthesized in two steps (Scheme 1) from dimethyl 2-fluoromalonate ester **5**, which was prepared from dimethyl 2-malonate ester by direct fluorination using fluorine gas using our previously reported conditions. [13] Michael addition of acrylonitrile gave the fluorocyanodiester **6b** [14] which could be readily decarboxylated to the target fluorocyanoester **4b** using Krapcho conditions by adapting a general literature procedure.[15] Alkylations of carbanions formed by deprotonation of dimethyl 2-fluoromalonate ester using sodium hydride by 4-bromobutyronitrile and bromovaleronitrile gave the corresponding alkylated products **6c** and **6d** respectively which could be decarboxylated by Krapcho processes to yield fluorocyanoester targets **4c** and **4d**. All intermediates **6b-d** and fluorocyanoester additives **4b-d** were isolated in very high purity by vacuum distillation leading to some product loss and corresponding relatively low yields. High purity material is, of course, essential when assessing overall additive performance in battery applications.

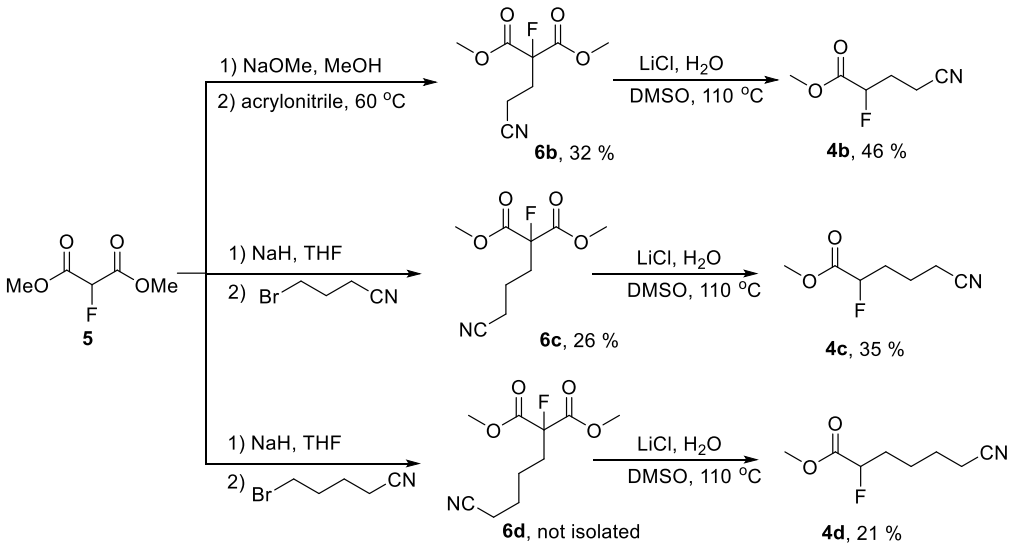

Scheme 1. Synthesis of fluorocyanoester additives **4b-d**

3.2 Reaction of fluorocyanoester additives **4b-d** in LIB cells

To establish the potential of using fluorocyanoester derivatives **4b-d** as additives for LIB electrolyte solutions, we evaluated the electrochemical reactivity of **4b-d** and their reaction pathways in LIB cells (Figure 2). During initial charge processes, electrolyte additives generally form SEIs, especially on the graphitic anode surface, which is important for improving the battery performance. [16] Since an SEI is formed by an irreversible charge consumption process during the first cycle of a graphite electrode, [17] cyclic voltammetry of the additives is useful to aid understanding of their contribution to the SEI formation process. To evaluate the electrochemical decomposition of the compounds to form an SEI on the graphitic anode, linear sweep voltammetry using CR2016 coin half cells with a metallic Li counter electrode was adopted in this study. We limited the charge rate of the cells to ensure that the overvoltage would be negligible and enable comparison and estimation of the relative reactivities of additives **4b-d**.

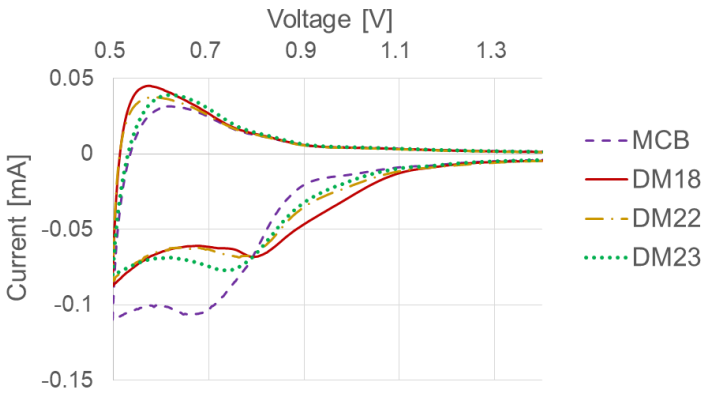

Figure 2. Cyclic voltammograms of graphite-metallic Li coin half cells, comparing the reduction potential of electrolyte solutions containing additives **4b-d**.

All the additives tested showed a reduction peak over 0.6V of Li coin halfcell potential. However no corresponding oxidation peaks were found on the reverse potential sweep, suggesting that the reductive pathways of the cyanoester additives are irreversible. Note that lithiation to the graphite anode started under 0.6V, and the oxidative delithiation current accordingly appears in the reverse scans. The reduction peak of F-MCB **4b** and related fluorocyanoesters F-MCP **4c** and F-MCH **4d** (Figure 2) was positively shifted compared to non-fluorinated MCB **4a**, which indicates that reduction of the fluoroesters was accelerated by the presence of the α-fluorine atom. The reduction is initiated by the carbonyl group accepting electrons, thereby generating a radical anion, exemplified by the comparative negative shift of the CV peak due to the carbonyl bond being more electron deficient due to inductive effects of the highly electronegative fluorine atom in the α-position.

In addition, the extent of the shift decreases as the length of connecting alkyl chain increases, indicating the contribution of the additional electron withdrawing effect of the pendent nitrile group that increases reduction potential as it becomes close to the ester functionality. Interestingly, the peak shift and float-swelling properties were even affected in the case of F-MCH **4d**, in which the cyano-moiety is located four carbon atoms away from the carbonyl functionality. This suggests that the cause of the shift is not only due to the inductive effect on the carbonyl group by fluorine and that all electronic effects need to be considered.

The enhanced reductivity induced by fluorination is confirmed by the additive consumption during the initial battery charge/discharge process. Table 1 shows the mass of each additive remaining in the electrolyte after the first charge/discharge process as determined by GC-MS. In contrast to the lack of reaction of the EC and PC solvent components during the initial charge/discharge process, the amount of VC and fluorinated cyanoester derivative decreased in the electrolyte solution. The decrease of VC was due to SEI formation reactions [18] and, similarly, the decrease of fluorinated cyanoesters was likely due to contributions to SEI formation. In contrast to the fluorinated additives, however, the MCB **4a** concentration was unchanged, indicating that MCB **4a** did not participate in an SEI formation reaction. Since the reduction peak position of MCB **4a** is negative compared to that of VC, it is presumed that the stable SEI was formed by VC before reaching the reaction potential of MCB **4a**. Therefore, MCB **4a** reduction did not proceed and remains unchanged in the electrolyte solution and does not contribute to the formation of an SEI layer.

Table 1. Mass retention of electrolyte components after initial charge/discharge cycle

Retention (Mass) after 1st charge/discharge cycle [%]				
Component/ Electrolyte solution	Without cyanoesters	F-MCP **4c**	F-MCB **4b**	MCB **4a**
Evaluated Additive	-	58	47	101
VC	27	30	24	26
EC	97	97	99	97

To characterize the product arising from reactions of the fluorocyanoester additives **4b-d**, NMR and XPS analysis was used to determine the composition of the anode SEI product formed during the initial charge/discharge processes. The composition of the anode SEI from a standard electrolyte solution containing carbonate solvents including EC has been reported to be a complex mixture which includes the reduction products of carbonate solvents, such as lithium ethylenedicarbonate (LEDC) from EC. [19-20] Such components can be eluted into D_2O and the SEI compositions can be indirectly determined by NMR analysis of D_2O extracts from the cycled electrodes. [21] As suggested by the electrolyte consumption analysis above, VC and fluorocyanoester additives **4b-d** are the main reactants during the initial charge/discharge process and, therefore, we focused on the contribution of these additives to SEI formation. D_2O extracts from the graphite anode after the 1st charge/discharge cycle were analyzed by ^1H NMR

spectroscopy (Figure 3). For ease of analysis, fully deuterated solvent EC-d_4 and PC-d_6 were used in the charge/discharge processes and extracts were analysed by NMR. This led to clear spectra where all the protons found in the extracted SEI components originated from the additives alone. We performed XPS analysis on the anode surface after the D_2O extraction process and confirmed that the graphite peak in the C1s spectrum remained after D_2O extraction as presented in Figure SI-7, suggesting that most of SEI had been extracted by the D_2O washing process.

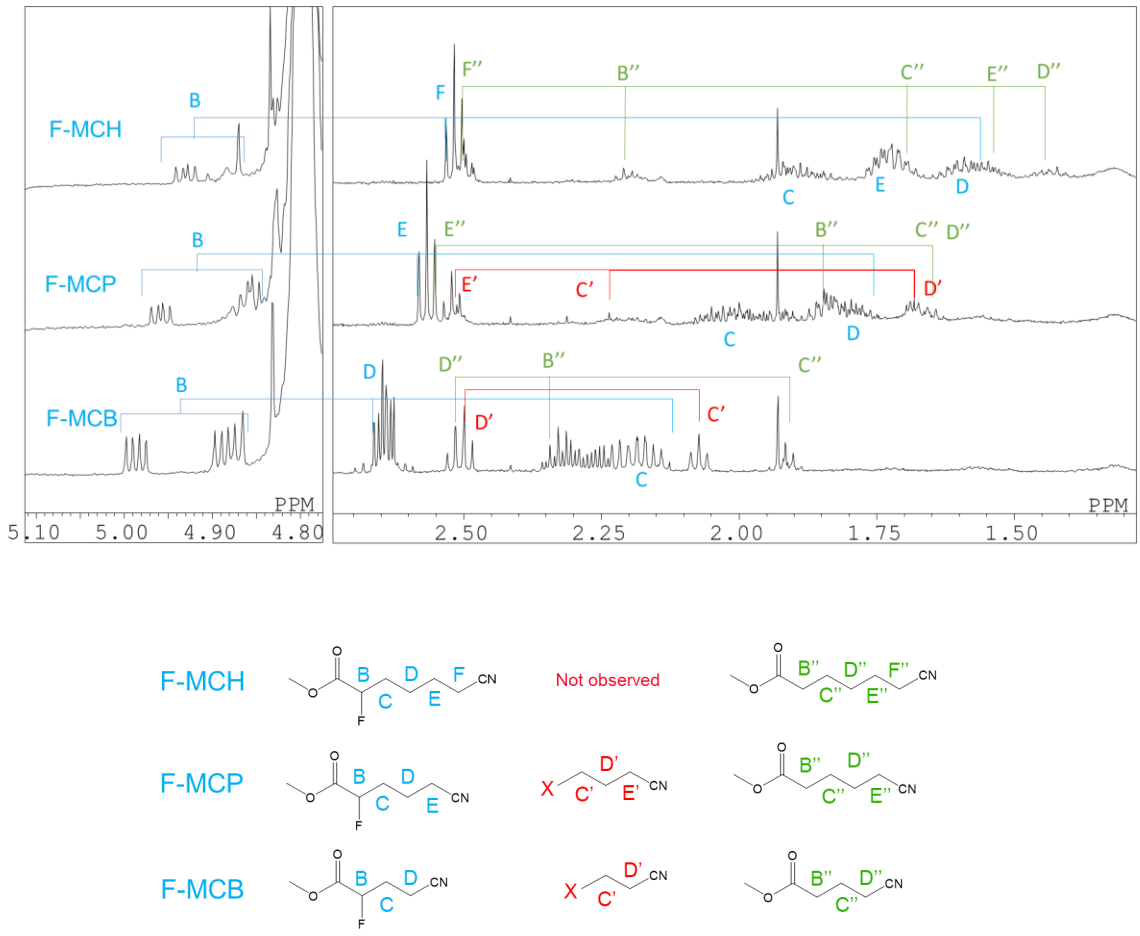

Figure 3. NMR spectra of D_2O extracts from the graphite anode after the 1st charge/discharge cycle of electrolyte solutions containing **4b-d**.

Figure 3 shows a comparison of NMR spectra of extracted anode SEI solutions arising from fluorocyanoester additives **4b-d**. The extracted solutions were analyzed by H-H COSY to aid peak assignment (indicated by a solid line connecting peaks on Figure 3, the detailed results are available in the Supporting Information as Figures SI-1 and SI-2). Based on this analysis, for the F-MCB **4b** system, three main components were extracted and observed; native reactant, defluorinated product and an SEI component. The native reactant and defluorinated product were also found in the washed solution, as shown in Figure SI-3 and SI-4. This suggests that they were possibly strongly adsorbed on the electrode surface and, therefore, less likely to be hydrolysis products associated with the SEI.

All the other resonances observed in Figure 3 are thought to be derived from the SEI. Anode SEIs that are composed of polycarbonates can be readily hydrolyzed with water, and as a result, polar monomer components can be eluted into D_2O. In this system, only the hydrolysis fragment originating from additives can be detected even if the additives reacted with EC-d_4 or PC-d_6 to form an SEI complex. The hydrolysis product in D_2O extracts from the cell with the electrolyte containing F-MCB **4b** consists of two carbon fragments, C' and D'. Based on the chemical shift, $H_{D'}$ was assigned to the carbon atom adjacent to the cyano-moiety due to the similarity of the chemical shift to that of $H_{D'}$ of F-MCB **4b**. Due to the wide range of possible chemical environments, C' cannot be definitively assigned, although it is likely to be bonded to a carbonyl group via a reaction with carbonate solvent and most likely generated through a hydrolysis pathway. Interestingly, the proton H_B was absent in the anode D_2O extracts. This was also confirmed by ^{19}F-NMR, where only native additives were found in addition to lithium fluoride, (Figure SI-5), produced by defluorination of the additive. In most cases the electrolytes contain

$LiPF_6$ and LiF is found as the major product resulting from salt reduction. [21] The presence of LiF was also confirmed in the ^{19}F-NMR spectrum of anode D_2O extract showing a singlet at -123 ppm due to LiF in addition to the signals arising from the native F-MCB and residual $LiPF_6$ (Figure SI-5). Such a hydrolysis component fragment was not observed in MCB **4a** extracted sample which suggests that the fluorination at the α-position causes the fluorocyanoester additive to fragment. Here we note that the same fragment was observed with standard EC and PC solvent (Figure SI-6).

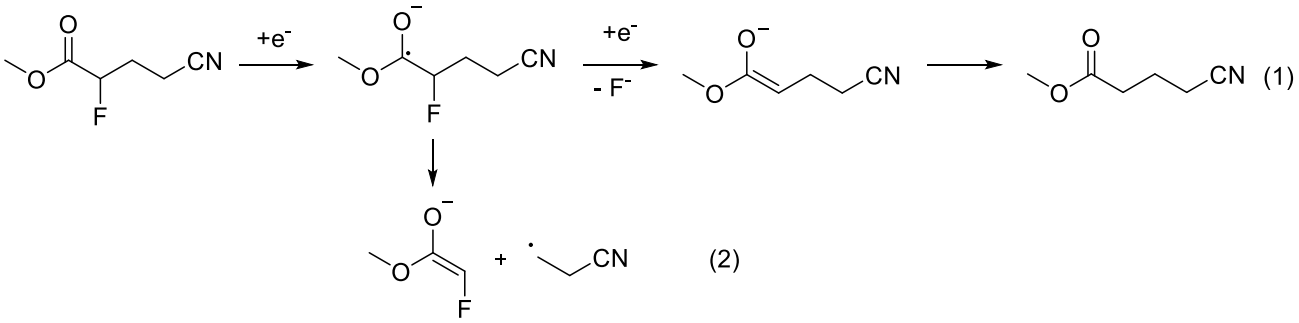

Scheme 2. Reduction pathway of fluorocyanoesters on graphite anode

Based on these experiments, the mechanism of reduction and decomposition of the fluorocyanoester additives on the graphite electrode is proposed in Scheme 2. The initial step is the carbonyl group accepting an electron forming a radical anion which then either undergoes either defluorination and subsequent protonation (pathway 1, Scheme 2) generating LiF and the corresponding defluorinated cyanoester. Alternatively, homolytic radical cleavage between the αβ position (pathway 2, Scheme 2) occurs and the resulting components are incorporated into the SEI similar to the SEI formation from EC.[22] There were no traces of fluorine containing organic

product either in the electrolyte or the anode D_2O extracts except LiF (Figure SI-5). The fluorocarbonate anion resulting from the homolytic radical cleavage was possibly further decomposed to generate fluoride anion.

Interestingly, from the analysis of the NMR spectra of the anode extracts, the products of pathway 2, Scheme 2 were found for additives F-MCB **4b** and F-MCP **4c**, but to a lesser extent for the longer alkyl chain compound F-MCH **4d**. Indeed, results suggest that the longer the alkyl chain of the compound, the more inhibited pathway 2, Scheme 2 is, to the extent that none of the expected products from this pathway are found for the longest chained F-MCH **4d**. Since the solubility of these fragments in D_2O is very likely, given the ready solubility of related adiponitrile ($C_4H_8(CN)_2$) in D_2O (see Figure SI-6), pathway 2 may affect the reduction peak at linear sweep voltammetry, making the initial reduction step kinetically unfavorable.

As lithium fluoride (LiF) formation was suggested in the NMR results for F-MCB **4b**, we further determined the anode and cathode surface composition by photoelectron spectroscopy. Figure 4 shows the XPS spectrum of C1s and F1s of the cathode and anode surface after the initial charge/discharge process.

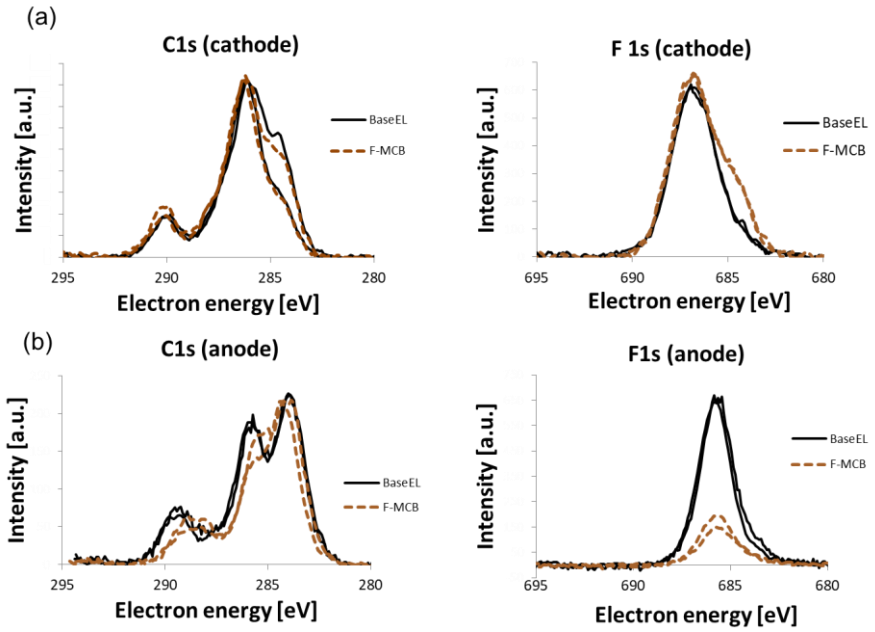

Figure 4. XPS spectra of C1s and F1s on the (a) cathode and (b) anode surface after initial charge/discharge process for electrolyte containing F-MCB **4b**.

In the F1s spectrum of the surface of the cathode, the peak at 686 eV is assigned to PVDF which is used as a binder and is present in all XPS spectra of the surfaces of cathodes. The PVDF peak due to the binder at the anode surface appeared weak in the electrolyte containing F-MCB **4b**, which is consistent with SEI formation at the anode. The enhanced shoulder around 684 eV was assigned to LiF. [23] The peak attributed to LiF was commonly present at the anode surface as shown by NMR analysis, but also at the cathode surface. Similar to the anode analysis, we extracted the SEI formed at the cathode and only the native component of the additives which might be adsorbed onto the cathode surface were observed. This suggested that the LiF may be present as a thin film on the surface. We carried out an LSV test with an LCO cathode half cell, but did not observe any obvious oxidation peaks before delithiation of LCO started around 3.6V. However, the charge-

discharge curve of the F-MCB electrolyte was resistively shifted at the early state of charge compared to that of the MCB and base electrolyte (Figure SI-9), which suggests that LiF formation arising from the F-MCB electrolyte happens at an early stage of the reduction process and simultaneously with delithiation from LCO. Whilst LiF can be formed on the cathode via decomposition of $LiPF_6$ over 4.2V (vs Li^+/Li), as suggested in a previous study,[24] here, the LiF formation should be promoted by fluoride ion or HF generated via pathway 1, Scheme 2. However, the details of cathode LiF formation from the fluorinated cyanoesters remains unclear at present.

The C1s spectrum of the anode surface formed using the electrolyte containing the F-MCB **4b** additive indicated that the alcoholic C-O and carbonate OCO peaks, at 286 eV and 290 eV respectively, shifted to a lower ratio to C-C at 284 eV. The enhanced carbonate carbon peak was due to the adsorbed F-MCB **4b**. This was consistent with the NMR result that the anode SEI formed from F-MCB **4b** contained a cyanoalkyl component in addition to the usual carbonate decomposition products. It was also confirmed that the C1s peak on the cathode assigned to carbonate moities was not affected by F-MCB **4b** addition. The peak at 284 eV was attributed to the carbon conductant present in the electrode.

3.3 Battery evaluation for gas suppression

In this study, aging tests were performed to assess the efficiency of additive compounds **4b-d** for battery-cell stability and reliability for long-term use. Accelerated tests are widely used to evaluate cells in a short time frame and typically carried out by heating and elevating at higher states of charge (SOC). Following typical conditions for commercial LIB testing, the assembled cells were continuously charged at 60 °C and 100% SOC, and the stability of the cells was evaluated by the

amount of swelling arising from gas generated by electrolyte decomposition. Swelling of the cell was measured by pouch cell thickness over the lifespan of testing. A comparison of cells with different additive components (1 wt%) allowed some understanding of the cause of gas production which could potentially lead to an effective way to suppress gas generation and the resulting swelling of commercial LCO/graphite batteries. Figure 5 shows the cell thickness resulting from cell swelling as a function of storage time keeping the cell at 60 °C and 4.45 V of constant charge voltage.

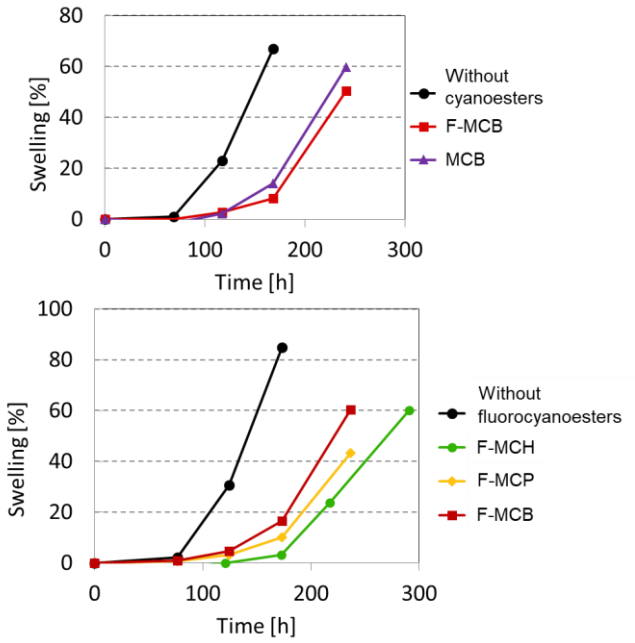

Figure 5. Swelling of battery cells as a function of CV charging time (t = 0 – 300 h).

In each case, the swelling rate of the cells was suppressed by addition of cyanoester MCB **4a** and the fluorocyanoester systems **4b-d** in comparison to the electrolyte solutions without these additives. Comparison of the charts for MCB **4a** and F-MCB **4b** show that α-fluorination decreases

swelling and the results for **4b-d** demonstrate that swelling decreases as the alkyl chain linking the fluoroester and nitrile functionalities increases.

Capacity retention is another measure of the stability during the test period and assesses the ability of a battery to retain stored energy. The capacity retention was defined as the ratio of discharge capacity after aging test to that of initial cycle. Capacity retention after 240 h (10d) is presented in Table 2 and the increased suppression of swelling with α-fluorination and longer cyanoalkyl chain was also established and increasing from 60 % to 66 % over the series. This indicates that the fluorocyanoesters provided some protection of the active materials, leading to higher discharge capacity retention.

Table 2. 0.2C discharge capacity retention after 240 h continuous charging

Additive compound	Capacity retention after 240 h aging[%]
MCB **4a**	60
F-MCB **4b**	64
F-MCP **4c**	65
F-MCH **4d**	66

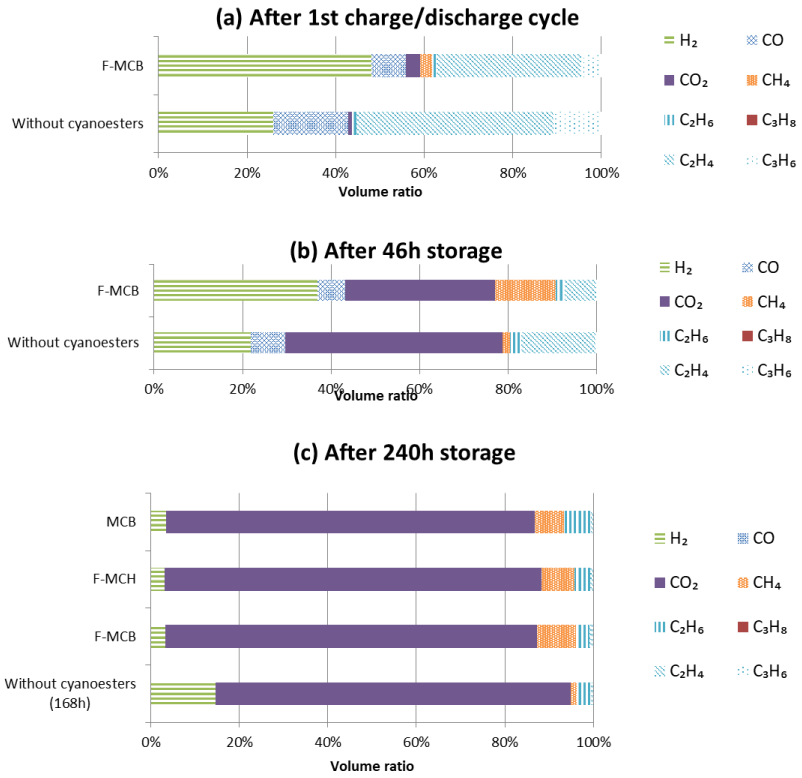

Figure 6. Composition of gas mixtures generated (a) during initial charge/discharge and (b) after 46 h continuous charging of two samples; F-MCB **4b** and VC, and neat VC. (c) Composition of gas mixtures generated after 240 h of four samples; F-MCB **4b** and VC, F-MCH **4d** and VC, MCB **4a** and VC, and neat VC.

The mechanism of gas suppression by the addition of fluorocyanoester derivatives to electrolyte solutions can be assessed based on the reaction products observed by NMR, GCMS and XPS. To investigate the origin of swelling, GC analysis was used to assess the composition of the gaseous products generated during the aging tests. Figure 6 shows the relative composition of gas mixtures generated in the cells during the tests. The data after the 1st charge/discharge cycle and 46 h were obtained for the cells where inert Ar was introduced to the pouch cell prior to battery operation in

order to allow easier extraction of small quantities of generated gas. The values shown are relative composition ratios of the volatile hydrocarbon gases (with less than four carbons) which can be separated by micro GC apparatus and does not correspond to the absolute value of the composition of the gas amount.

The most significant change of the gas mixture compositions formed during the charging test was CO_2 generation which is the main contribution to cell swelling. Oxidative degradation of EC on charged LCO surfaces leading to CO_2 generation has been reported in many studies. [25-27] As discussed above, the addition of cyanoester additives suppressed cell swelling in continuous charging, which means CO_2 generation was suppressed. Such CO_2 suppression is commonly found upon addition of alkyl nitrile compounds to electrolyte [28,29] and it has been proposed that nitriles could stabilize the LCO surface due to chemisorbtion. In our cell, the gas suppression effect of additives relative to electrolyte is due to suppression of solvent decomposition by the nitrile group of MCB **4a** or F-MCB **4b**. As discussed in the initial process, reactions of fluorocyanoester additives **4b-d** could provide LiF on the cathode surface. It has been reported that LiF provides a similar protective effect on a cathode[30-32] and so the fluorinated cyanoesters could provide additional CO_2 suppression effects via LiF formation on the cathode in addition to the contribution by the chemisorbed nitrile groups.

In addition to CO_2 generation, hydrogen (H_2) and some hydrocarbons including ethylene (C_2H_4) and methane (CH_4) were found upon the initial charge and discharge cycle test, as well as during the aging tests. Ethylene (C_2H_4) and hydrogen (H_2) in the initial charge and discharge cycle were commonly observed and are known to be generated as a result of reduction of EC.[33] The amount of CH_4 gradually increased significantly upon F-MCB **4b** addition rather than when the non-fluorinated additive MCB **4a** was used. The CH_4 is product of reductions of both F-MCB **4b** and

MCB **4a** additives. It is reasonable that CH_4 is formed by loss of a methyl radical by the pathway 3, Scheme 3 by which the methyl radical derives from the radical anion that is formed by initial reduction of the carbonyl group. The ^{1}H-NMR is inconclusive in confirming this process due to the expected peak position overlapping with the deuterated solvent impurity MeOD. The gas generation analysis, however, suggests that pathway 3, Scheme 3 should be considered as a further degradation process of the additive. Based on these findings, three competing reactions arising from F-MCB **4b** reduction contribute to the battery aging process with continuous charging and suggests that the additive component reacts similarly in the first charge/discharge cycle.

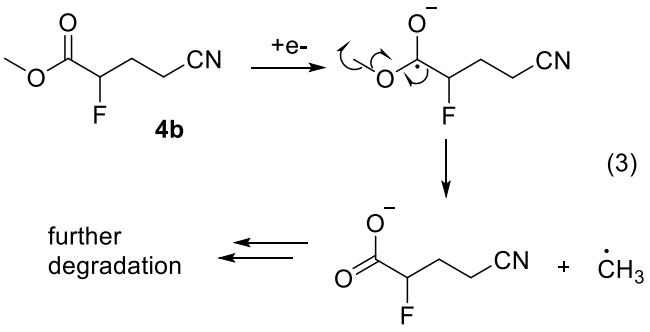

Scheme 3. Loss of methyl radicals from fluorocyanoester additives upon reduction

The contribution by the fluorocyanoester additives **4b-d** to cathode protection was also observed in AC impedance measurements. Figure 7 shows the Cole-Cole plots of the assembled cells at initial charging and after the continuous charging test (240 h). Two semicircles are present in the Cole-Cole plot more obviously in the 240 h charging tests. Cole-Cole plot of LCO/graphite pouch cell with VC and SN containing electrolyte was reported in previous study where the semi-circle in the lower frequency region is due to the charge transfer resistance of the LCO cathode and the charge transfer resistance was increased during cycling.[34] Charge-transfer resistance is sensitive

to active material surface and affected by SEI or protective layer formation. After the initial charge, fluorocyanoester additives **4b-d** increase the semi-circles at low frequency, suggesting LiF formation on the cathode. After 240 h tests, the semicircles of cathode charge-transfer resistance decreased as the carbon chain length between the fluoroester group and nitrile group increases. This trend reflects cell-swelling suppression and capacity recovery with the introduction of fluorocyanoester additives **4b-d**. In addition to electrolyte decomposition during continuous charging, cathode degradation producing free cobalt in the solution also occurred. [35] For voltages greater than 4.2 V, the capacity fading scaled with the measured amount of cobalt dissolution which was found to correlate with structural changes of LCO. [36] A cathode protection effect of fluorocyanoester additives **4b-d** may suppress such degradation of the LCO as well as contributing to the suppression of electrolyte decomposition during the continuous charging process which is enhanced in the longer carbon chain cyanoalkyl additives providing stable anode SEI as discussed above.

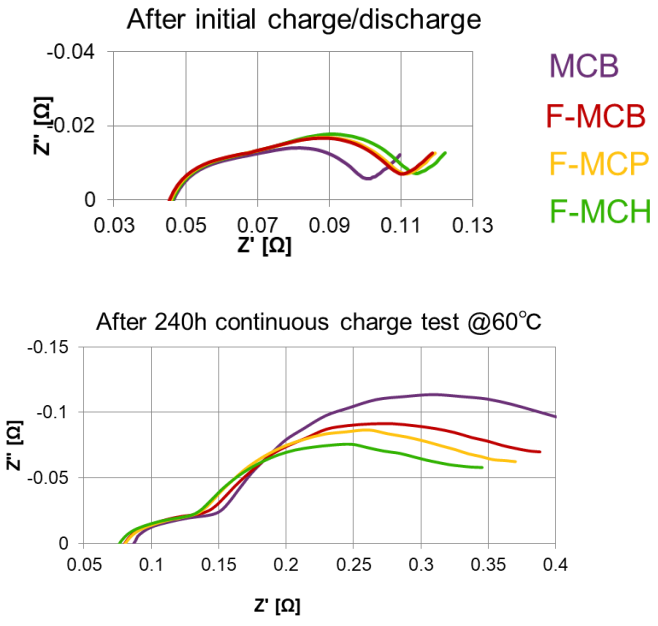

Figure 7. Cole-Cole plot at the fully charged state.

Consumption of the additives during the aging test provides another insight into understanding battery improvement. Table 3 shows the consumption of electrolyte components after a 240 h continuous charge test where the electrolyte taken from the cell was analyzed in a similar way to the analysis of the initial charge/discharge process described above. As shown in Table 3, the trend of additive consumption reflects the ease of additive reduction, suggesting that reduction of the additives continues during the 60 °C charging test. As discussed in the previous section, fluorocyanoesters **4b-d** engage in SEI formation via generation of cyanoalkyl radicals (pathway 2, Scheme 2). However, such decompositions result in monofunctional radical components that could initiate or terminate SEI polymerization processes and are not able to propagate the polymer chain upon further reaction with carbonates. Hence, the degree of propagation of SEI is suggested to decrease according to the extent of pathway 2, Scheme 2. As a result, longer cyanoalkyl additives would form stable SEIs involving a higher contribution of carbonate solvents which consequently prevent further decomposition of additives during the aging process. Hence, the longer alkyl fluorocyanoesters can increase gas production by pathway 3, Scheme 3 in contrast to the shorter alkyl fluorocyanoesters which only partially contribute to swelling reduction.

Table 3. Mass retention of additives after 240 h continuous charging test

Retention (Mass) after 240 h continuous charging test [%]			
Component/ Electrolyte solution	F-MCP **4c**	F-MCB **4b**	MCB **4a**
Evaluated Additive	12	8	17
VC	0	0	0
EC	93	94	94

4. CONCLUSIONS

Synthesis of a range of fluorocyanoester derivatives **4b-d** from dimethyl 2-fluoromalonate ester **5** was established using Michael, alkylation and Krapcho reactions as appropriate. The fluorocyanoesters **4b-d** are effective additives in LIB electrolytes and, upon addition of 1 wt% additive to the electrolyte, significantly reduce swelling in the cells over 300 h periods as well as capacity retention during the aging test.

The role played by the fluorocyanoester additives **4b-d** in battery performance is multi-faceted and were explored by linear sweep cyclic voltammetry, NMR, GCMS and XPS techniques. Cyclic voltammetry showed that reduction of the carbonyl group occurs initially and this is enhanced by the presence of an electron withdrawing α-fluorine atom and the relative proximity of the nitrile

group as would be expected. Following formation of the radical anion by reduction, three possible degradation processes of the fluorocyanoester additives are most likely: loss of fluoride ion, loss of methyl radicals and cleavage of the αβ carbon-carbon bond (Schemes 2 and 3). Each process would affect battery performance and evidence for each process has been observed.

Loss of fluoride ion (pathway 1, Scheme 2) was exemplified by the observation of LiF by ^{19}F NMR and XPS and this would enhance protection of the cathode in addition to chemisorbtion of the nitrile moiety of the additives, leading to improved cell swelling and capacity retention during aging tests. Cleavage of the αβ carbon-carbon bond (pathway 2, Scheme 2) was inferred by NMR spectroscopic analysis of the SEI surface extracts and would enable SEI formation on the anode via initiation of free radical polymerization processes. Loss of methyl radicals (Pathway 3, Scheme 3) was inferred by the observation of methane gas in the mixture of gases generated in the cells which would contribute to swelling of the cells.

Overall, therefore, electrode protection upon addition of fluorocyanoesters **4b-d** to the electrolyte is the main contribution to the improvement of battery stability for these additives but improvements on the electrode protection are offset by free radical processes initiated at the anode; the longer alkyl fluorocyanoesters showed the best improvement with effective cathode protection. Consequently, design of electrolyte additives must, therefore, take into account contrasting battery performance effects.

ASSOCIATED CONTENT

The following file is available free of charge.

Synthetic procedures for the preparation of **4,6**, NMR spectra of **4,6** and further NMR data (PDF).

AUTHOR INFORMATION

Corresponding Authors

* E-mail: takumi.hiasa@murata.com; graham.sandford@durham.ac.uk

ORCHID

Graham Sandford 0000-0002-3266-2039

Author Contributions

The manuscript was written through contributions of all authors. All authors have given approval to the final version of the manuscript.

REFERENCES

(1) *https://www.marketresearchengine.com/lithium-ion-battery-market1* (accessed May 2019).

(2) Cho, J.; Jeong, S.; Kim, Y. Commercial and Research Battery Technologies for Electrical Energy Storage Applications. *Prog. Energy Combust. Sci.* **2015**, *48*, 84 − 101.

(3) Zuo, X.X.; Fan, C.J.; Xiao, X.; Liu, J.S.; Nan, J.M. High-voltage Performance of LiCoO2/graphite Batteries with Methylene methanedisulfonate as Electrolyte Additive. *J. Power Sources* **2012**, *219*, 94 - 99.

(4) Xia, L.; Xia, Y.; Liu, Z. Thiophene Derivatives as Novel Functional Additives for High-voltage LiCoO2 Operations in Lithium Ion Batteries. *Electrochimica Acta* **2015**, *151*, 429 - 436.

(5) Zhao, M.; Zuo, X.; Ma, X.; Xiao, X.; Yu, L.; Nan, J. Diphenyl Disulfide as a New Bifunctional Film-forming Additive for High-voltage $LiCoO_2$/graphite Battery Charged to 4.4 V. *J. Power Sources*, **2016**, *323*, 29 – 36.

(6) Kim, G.; Dahn, J. R. The Effect of Some Nitriles as Electrolyte Additives in Li-Ion Batteries. *J. Electrochem. Soc.* **2015**, *162*, 437 – 447.

(7) Abu-lebdeh, Y.; Davidson, I. New Electrolytes Based on Glutaronitrile for High energy/power Li-ion Batteries. *J. Power Sources*, **2009**, *189*, 576 – 579.

(8) Abu-lebdeh, Y.; Davidson, I. High-Voltage Electrolytes Based on Adiponitrile for Li-Ion Batteries. *J. Electrochem. Soc.* **2009**, 60 – 65.

(9) Aurbach, D.; Levi, M. D.; Levi, E; Schechter, A. Failure and Stabilization Mechanisms of Graphite Electrodes. *J. Phys. Chem. B* **1997**, *101*, 2195 – 2206.

(10) Minato, T.; Abe T. Surface and Interface Sciences of Li-ion Batteries: -Research Progress in Electrode–Electrolyte Interface. *Progress in Surface Science* **2017**, *92*, 240-280.

(11) Sun, X.G.; Liao, C.; Baggetto, L.; Guo, B.; Unocic, R. R.; Veith, G. M.; Dai, S. Bis(fluoromalonato)borate (BFMB) Anion Based Ionic Liquid as an Additive for Lithium-ion Battery Electrolytes. *J. Mater. Chem. A* **2014**, *2*, 7606 – 7614.

(12) Lyu, H.; Li, Y.; Jafta, C. J.; Bridges, C. A.; Meyer, H.M.; Borisevich, A.; Paranthaman, M.P.; Dai. S.; Sun, X. G. Bis(trimethylsilyl) 2-fluoromalonate Derivatives as Electrolyte Additives for High Voltage Lithium Ion Batteries. *J. Power Sources* **2019**, *412*, 527 – 535.

(13) Harsanyi, A.; Sandford, G. Fluorine Gas for Life Science Syntheses: Green Metrics to Assess Selective Direct Fluorination for the Synthesis of 2-Fluoromalonate esters. *Green Chem.* **2015**, *17*, 3000 - 3009.

(14) Willis, N.J.; Fisher, C.A.; Alder, C.M.; Harsanyi, A.; Shukla, L.; Adams, J.P.; Sandford, G. Sustainable Synthesis of Enantiopure fluorolactam Derivatives by a Selective Direct Fluorination – Amidase Strategy. *Green Chem.* **2016**, *18*, 1313 - 1318.

(15) Krapcho, A.P.; Weimaster, J.F.; Eldridge, J.M.; Jahngen, E.G.E.; Lovey, A.J.; Stephens, W.P. Synthetic Applications and Mechanism Studies of the Decarbalkoxylations of Geminal Diesters and Related Systems Effected in Dimethyl Sulfoxide by Water and/or by Water with Added Salts. *J. Org. Chem.* **1978**, *43*, 138 – 147.

(16) Verma, P.; Maire, P.; Novák, P. A Review of the Features and Analyses of the Solid Electrolyte Interphase in Li-ion Batteries. *Electrochimica Acta* **2010**, *55*, 6332 - 6341.

(17) Aurbach, D.; Markovsky, B.; Levi, M.D.; Levi, E.; Schechter, A.; Moshkovich, M.; Cohen, Y. New Insights into the Interactions between Electrode Materials and Electrolyte Solutions for Advanced Nonaqueous Batteries. *J. Power Sources*, **1999**, *81/82*, 95 - 111.

(18) Aurbach, D.; Gamolsky, K.; Markovsky, B.; Gofer, Y.; Schmidt, M.; Heider, U. On the Use of Vinylene Carbonate (VC) as an Additive to Electrolyte Solutions for Li-ion Batteries. *Electrochimica Acta* **2002**, *47*, 1423 - 1439.

(19) Aurbach, D. Review of Selected Electrode–Solution Interactions which Determine the Performance of Li and Li Ion Batteries. *J. Power Sources* **2000**, *89*, 206 - 218.

(20) Xu, K.; Zhuang, G.V.; Allen, J.L.; Lee, U.; Zhang, S.S.; Ross, P.N.; Jow, T.R. Syntheses and Characterization of Lithium Alkyl Mono- and Dicarbonates as Components of Surface Films in Li-Ion Batteries. *J. Phys. Chem. B* **2006**, *110*, 7708 - 7719.

(21) Nie, M.; Chalasani, D.; Abraham, D. P.; Chen, Y.; Bose, A.; Lucht, B. L. Lithium Ion Battery Graphite Solid Electrolyte Interphase Revealed by Microscopy and Spectroscopy. *J. Phys. Chem. C* **2013**, *117*, 1257 − 1267.

(22) Shkrob, I.A.; Zhu, Y.; Marin, T.W.; Abraham, D. Reduction of Carbonate Electrolytes and the Formation of Solid-Electrolyte Interface (SEI) in Lithium-Ion Batteries. 1. Spectroscopic Observations of Radical Intermediates Generated in One-Electron Reduction of Carbonates. *J. Phys. Chem. C* **2013**, *117*, 19255 − 19269.

(23) Verma, P.; Maire, P.; Novák, P. A Review of the Features and Analyses of the Solid Electrolyte Interphase in Li-ion Batteries. *Electrochimica Acta* **2010**, *55*, 6332 – 6341.

(24) Leroy, S.; Blanchard, F.; Dedryvere, R.; Martinez, H.; Carre, B.; Lemordant, D.; Gonbeau, D. Surface Film Formation on a Graphite Electrode in Li-ion Batteries: AFM and XPS Study. *Surf. Interface Anal.* **2005**, *37*, 773 –781.

(25) Park, J. H.; Chou, J. H.; Kim, J. S.; Shim, E. G.; Lee, S. Y. High-voltage Cell Performance and Thermal Stability of Nanoarchitectured Polyimide Gel Polymer Electrolyte-coated $LiCoO_2$ Cathode Materials. *Electrochimica Acta* **2012**, *86*, 346 − 351.

(26) Liu, D. Q.; Qian, K.; He, Y. B.; Luo, D.; Li, H.; Wu, M. Y.; Kang, F. Y.; Li, B. H. Positive Film-forming Effect of Fluoroethylene Carbonate (FEC) on High-voltage Cycling with Three-Electrode $LiCoO_2$/Graphite Pouch Cell. *Electrochimica Acta* **2018**, *269*, 378 − 387.

(27) Tebbe, J.L.; Fuerst T.F.; Musgrave C.B. Degradation of Ethylene Carbonate Electrolytes of Lithium Ion Batteries via Ring Opening Activated by $LiCoO_2$ Cathode Surfaces and Electrolyte Species. *ACS Appl. Mater. Interfaces* **2016**, *8*, 26664 - 26674.

(28) Kim, Y.S.; Lee, H. C.; Song, H.-K. Surface Complex Formation between Aliphatic Nitrile Molecules and Transition Metal Atoms for Thermally Stable Lithium-Ion Batteries. *ACS Appl. Mater. Interfaces* **2014**, *6*, 8913 − 8920.

(29) Chen, R. J.; Liu, F.; Chen, Y.; Ye, Y. S.; Huang, Y. X.; Wu, F.; Li, L. A. An Investigation of Functionalized Electrolyte Using Succinonitrile Additive for High Voltage Lithium-ion Batteries. *J. Power Sources* **2016**, *306*, 70 − 77.

(30) Xiong, X.; Wang, Z.; Yin, X.; Guo, H.; Li, X. A Modified LiF Coating Process to Enhance the Electrochemical Performance Characteristics of $LiNi_{0.8}Co_{0.1}Mn_{0.1}O_2$ Cathode Materials. *Mater. Lett.* **2013**, *110*, 4 – 9.

(31) Sun, Y.; Lee, H.W.; Zheng, G.; Seh, Z. W.; Sun, J.; Li, Y.; Cui, Y. In Situ Chemical Synthesis of Lithium Fluoride/Metal Nanocomposite for High Capacity Prelithiation of Cathodes. *Nano Lett.* **2016**, *16*, 1497 - 1501.

(32) Liu, K.; Zhang, Q.; Dai, S.; Li, W.; Liu, X.; Ding, F.; Zhang, J. Synergistic Effect of F–Doping and LiF Coating on Improving the High-Voltage Cycling Stability and Rate Capacity of

$LiNi_{0.5}Co_{0.2}Mn_{0.3}O_2$ Cathode Materials for Lithium-Ion Batteries. *ACS Appl. Mater. Interfaces* **2018**, *10*, 34153 - 34162.

(33) Tasaki, K.; Kanda, K.; Kobayashi, T.; Nakamura, S.; Ue, M. Theoretical Studies on the Reductive Decompositions of Solvents and Additives for Lithium-Ion Batteries near Lithium Anodes Batteries, Fuel Cells, and Energy Conversion. *J. Electrochem. Soc.* **2006**, *153*, A2192.

(34) Kim, G.Y.; Petibon, R.; Dahn, J. R. Effects of Succinonitrile (SN) as an Electrolyte Additive on the Impedance of $LiCoO_2$/Graphite Pouch Cells during Cycling Batteries and Energy Storage. *J. Electrochem. Soc.* **2014**, *161*, A506 - A512.

(35) Vetter, J.; Novak, P.; Wagner, M.R.; Veit, C.; Moller, K.C.; Besenhard, J.O.; Winter, M.; Wohlfahrt-Mehrens, M.; Vogler, C.; Hammouched, A. Ageing Mechanisms in Lithium-ion Batteries. *J. Power Sources* **2005**, *147*, 269 – 281.

(36) Amatucci, G. G.; Tarascon, J. M.; Klein, L. C. Cobalt Dissolution in $LiCoO_2$-based Non-aqueous Rechargeable Batteries. *Solid State Ionics* **1996**, *83*, 167–173.